Taylor & Francis
Taylor & Francis Group

Welding International

ISSN: 0950-7116 (Print) 1754-2138 (Online) Journal homepage: http://www.tandfonline.com/loi/twld20

Influence of welding position and parameters in orbital tig welding applied to low-carbon steel pipes

Daniel Wallerstein Figueirôa, Ivan Olszanski Pigozzo, Régis Henrique Gonçalves e Silva, Tiago Felipe de Abreu Santos & Severino Leopoldino Urtiga Filho

WELDING INTERNATIONAL, 2017
http://dx.doi.org/10.1080/09507116.2016.1218615

Taylor & Francis
Taylor & Francis Group

Influence of welding position and parameters in orbital tig welding applied to low-carbon steel pipes

Daniel Wallerstein Figueirôa[a], Ivan Olszanski Pigozzo[b], Régis Henrique Gonçalves e Silva[b], Tiago Felipe de Abreu Santos[a] and Severino Leopoldino Urtiga Filho[a]

[a]Mechanical Engineering Department, Universidade Federal de Pernambuco – UFPE, Recife, Brazil; [b]Welding Laboratory – LABSOLDA, Welding and Mechatronics Institute, Universidade Federal de Santa Catarina – UFSC, Florianópolis, Brazil

ABSTRACT

The most notable characteristic of Orbital TIG welding is the constant geometric profile of the tubes. In the context of orbital TIG welding of tubes with a large diameter and thick walls, the relationship between the welding position, the use of constant or pulsed current and also the value of the average current on the geometric characteristics of the beads obtained was studied. We deposited welds on SAE 1020 carbon steel tubes, as well as taking macrographs of the cross-sections of the beads using optical microscopy. High-definition films were used to understand the behaviour of the weld pool in different welding positions. The geometric characteristics were quantified using macrographs and software, and the relationship between these characteristics and the above-mentioned variables were traced. In addition, an analysis of the microstructure of the samples was carried out, correlating with Vickers microhardness. It was concluded that the beads welded with pulsed current were more reinforced and wider, as well as being harder and having a finer microstructure. The vertical up position resulted in beads with a lower shape factor and more penetration, and the overhead position resulted in beads with a low shape factor.

KEYWORDS

Welding position; orbital TIG; penetration; shape factor

1. Introduction

In recent years, the number of proven reserves of oil and natural gas in Brazil has been constantly increasing [1]. This sharp increase in reserves has called for pipelines to be built to transport crude oil and its derivatives. Building these pipelines is expensive, mainly owing to the time it takes to build them [2]. Orbital TIG welding is a process for welding tubes which provide quality, reproducibility and productivity [3]. In this process, the welding torch is positioned, so that it follows the geometric profile of the tubes to be welded, which remain stationary [3,4]. This configuration leads to a characteristic that is specific to orbital welding: the welding position constantly changes during the process, which means that studies on the effect of the position are vital for successful application. Orbital welding can be carried out with relatively high welding speeds and can be performed in environments where space is limited, as well as ensuring that defects are kept to a minimum, since the process is automated [4–8].

Like the oil and gas sector, this process can be applied in the aerospace sector, since there is a great deal of responsibility for welds subjected to high pressures, which means that a high level of quality and reproducibility is necessary, which is difficult to obtain via manual welding processes [9–12].

The aim of this work is to study the influence of welding positions, the average current and the use of constant or pulsed current on the geometric characteristics of beads, such as reinforcement, width, penetration and shape factor, as well as to carry out a microstructural analysis.

2. Materials and methods

For orbital TIG welding, SAE 1020 low-carbon steel tubes with a diameter of 16″ (406.4 mm) and a thickness of 1/2″ (12.7 mm) were used, separated into rings with a width of approximately 200 mm. The filler wire used was AWS ER70S-6 with a diameter of 1.2 mm and we used argon shielding gas with 99.99% purity. The typical chemical compositions of the base material and the filler wire (quality certified) are provided in Table 1. We used an IMC Digi PLUS A7 power supply, a TIG Abicor Binzel series AUT-WIG 400 W torch and an EW Ce-2 tungsten electrode, with a diameter of 3.2 mm and sharpening angle of 30°.

Selected from Soldagem & Inspeção 2015 20(4) 446–455.

Table 1. Typical chemical composition of the base metal and the filler wire (%. p.).

	C	Mn	Si	P	S	Ni	Cr	Mo	V	Cu
Base metal	0.17–0.23	0.30–0.60	–	0.04 max	0.050 max	–	–	–	–	–
Filler wire (AWS ER70S-6)	0.09	1.47	0.91	0.012	0.13	–	–	–	–	0.22

Table 2. Parametrization of tests with constant current and pulsed current.

Constant current (CC)			Pulsed current (PC)					
I (A)	U (V)	v_a (m·min^{-1})	I_m (A)	I_p (A)	I_b (A)	U_p (V)	U_b (V)	$v_{a,p}$ (m·min^{-1})
120	10.4	0.9	120	160	80	11.3	10.3	1.1
140	10.9	1.1	140	187	93	11.2	10.2	1.6
160	11.3	1.3	160	213	107	11.3	10.4	1.8

Notes: I is the welding current, U is the voltage and v_a is the feed rate for the wire. The label m means average, p refers to the pulse, and b refers to the base.

The methodology involved constructing a static characteristic curve via preliminary tests, in order to find possible systematic errors in the power supply and primarily to find the reference voltage of the *Automatic Voltage Control* (AVC). Next, tests were performed in order to determine a wire speed/power (ws/Pow) ratio that ensures that the filler metal is continuously fed into the weld pool. In the case of a non-continuous feed (in the case of detachments), the feed rate was increased (therefore increasing the ws/Pow ratio). On the other hand, when the wire reached the weld pool when still solid, the feed rate was decreased (decreasing the ws/Pow ratio). The ideal continuous feeding characteristic was found empirically between these two above-mentioned limits. The ratio was calculated using Equation 1 given below:

$$\left(v_a/\text{Pot}\right) = 60 \times v_a/\text{Pot} \qquad (1)$$

where (v_a/Pot [wire speed/Pow]) is the ratio between the wire speed/power, to be calculated, in units of [m·J^{-1}], v_a (wire speed) is the feed rate of the wire in [m·min^{-1}] and Pot (power) is the power of the arc in [W].

Once the preliminary tests had been performed, weld beads were deposited on the tubes, in four separate welding positions (vertical up, flat, vertical down and overhead), and using different welding voltage values, including the use of constant and pulsed current. The parametrization used can be found in Table 2.

The weld pool in the different welding positions was studied using a Canon 60D digital camera with a lens from the same brand, reference EF 180mm F/4L macro, fitted with a 650 nm bandpass filter.

The metallographic preparation of the samples for macrographs and micrographs involved sanding with wet sandpaper with granulometric distributions of 320, 400, 600 and 1200 mesh, followed by polishing with diamond paste with a granulometric distribution of 1 μm. The micrographs were taken after chemical etching with Nital 3% using an Olympus optical microscope, model BX51M and the software for image capture and analysis was Analysis 5.1. For the micrographic analysis, chemical etching with Nital 6% was used. The geometric characteristics, as shown in Figure 1, were measured using *ImageJ* software. As well as the geometric characteristics shown in Figure 1, the shape factor was calculated,

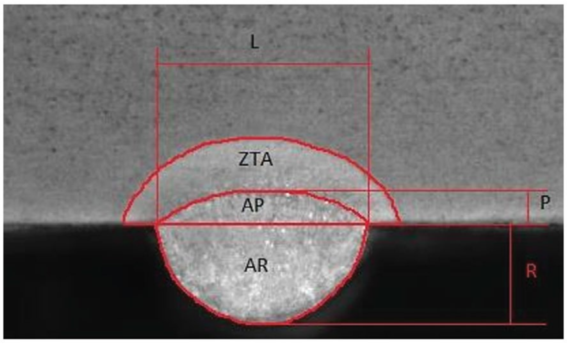

Figure 1. Geometric characteristics measured on macrographs.
Notes: L = width of bead; ZTA = heat-affected zone; AP = penetration zone; P = linear penetration; AR = reinforcement zone; R = linear reinforcement.

defined as the ratio between width and reinforcement of the cross-section of the bead.

Vickers microhardness tests were performed, using the Insize microhardness tester, model ISH – TDV 1000, with a diamond indenter with a square base and angle of 136°. A force of 500 gf was used and the residence time was 15 s. Indentations were carried out from the base metal in the direction of the fusion zone at intervals of 0.5 mm between each one.

3. Results and discussion

Preliminary tests were used to find a ws/Power ratio that would guarantee a continuous feed of metal. The ratio found was of the order of 1.2×10^{-5} m·J^{-1}, with variations of less than 3.4% between the welding positions. Taking into account the resolution of the wire tensioner used for the work (0.1 m·min^{-1}), it can be noted that a constant ws/Pow ratio was found for all the welding positions. This ratio was used in subsequent tests and successfully kept the filler metal feed stable, which is a very significant result in terms of technology, since we can use the ws/Pow ratio to find a suitable feed rate for a given welding current.

It is important to emphasize that parametrizations that lead to a low ws/Pow ratio result in non-continuous metal transfer, which in turn creates beads with a significantly lower shape factor (beads with low wettability). This was noticed during the preliminary tests, by doing comparative analyses between the data acquisition on voltage and the geometry of the weld beads. Non-continuous transfer

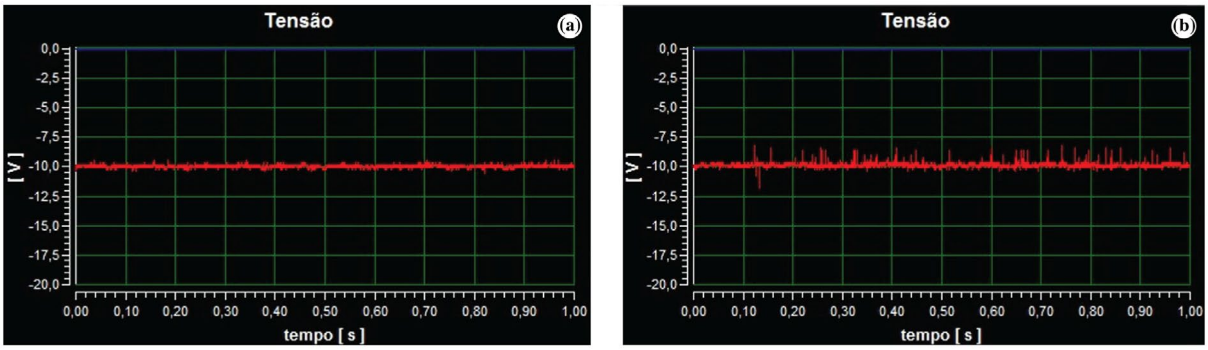

Figure 2. Voltage signal for (a) continuous and (b) non-continuous metal transfers.
Note: Tensao = voltage; tempo = time.

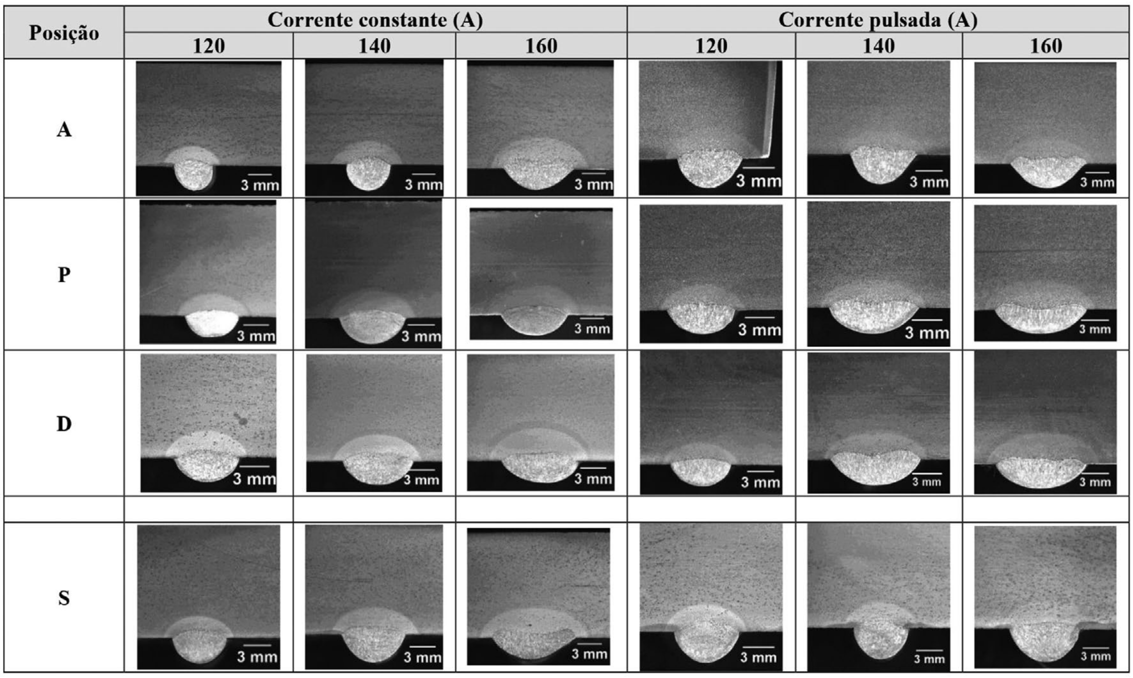

Figure 3. Macrographs of the cross-section of weld beads performed with constant current and pulsed current.
Note: Posicao = position; Corrente constant = constant current; Corrente pulsada = pulsed current.

is easy to spot on the voltage oscillogram as a variation in this parameter is shown, in the form of a noise that has a larger amplitude than the background noise that is always present when the power supply is functioning. Since the arc voltage is proportional to its length, the authors believe that the non-continuous transfer is linked to a variation in the energized length of the arc, which is first directly connected to the weld pool (moment when a drop detaches, linked to a longer energized arc length), then goes up or 'scales' the filler wire (the moment after detachment, leading to a shorter length). This variation in the energized arc length was prevented when the ws/Pow ratio was adjusted to the values that guarantee a continuous metal feed. This behaviour was noticed using films made during the study. The variations in the voltage signal can be seen in Figure 2, which shows (a) voltage acquisition for a bead with suitable ws/Pow ratio and (b) an oscillogram for a low ws/Pow ratio.

Figures 3–5 relate to the main geometric characteristics measured in the study. Figure 3 shows the

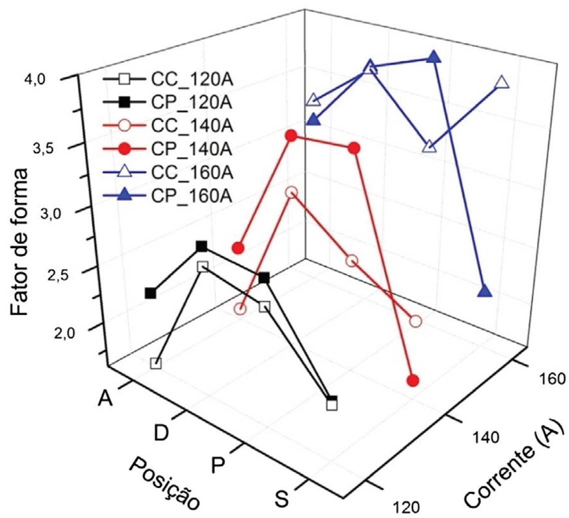

Figure 4. Shape factor depending on the welding position and current.
Notes: Fator de forma = shape factor; Posicao = position; Corrente = current.

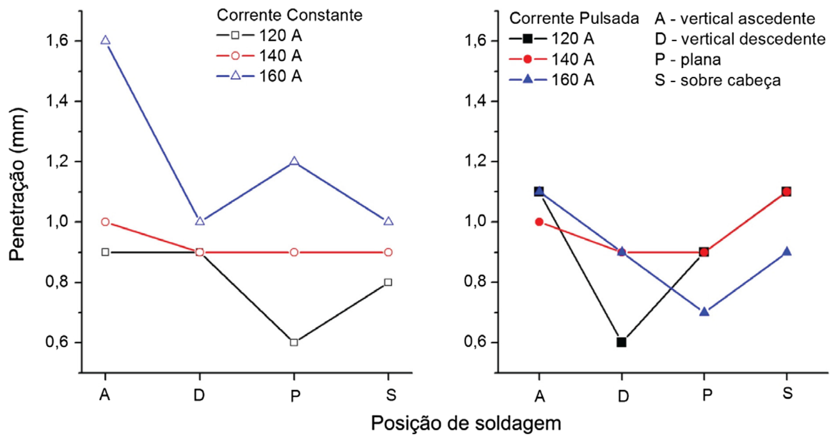

Figure 5. Penetration depending on the welding position for constant current and pulsed current.
Note: Penetração = penetration; Posição de soldagem = welding position; Corrente constant = constant current; Corrente pulsada = pulsed current; A – vertical up; D – vertical down; P – flat; S – overhead.

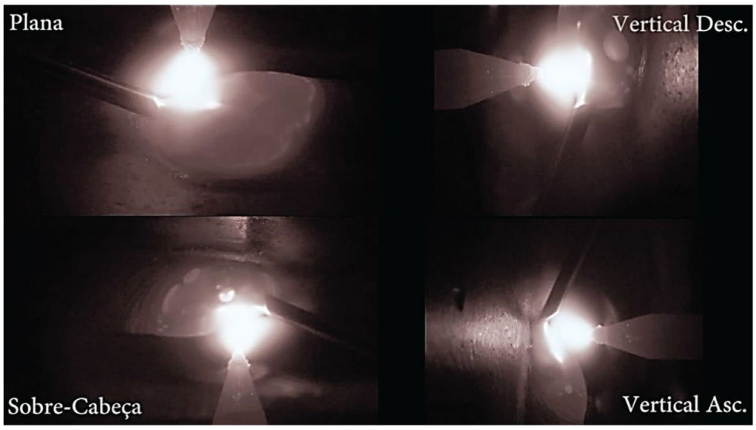

Figure 6. Stills taken from films in the four welding positions.
Note: Plana = flat; Vertical asc = vertical up; Sobre-cabeca = overhead; Vertical desc = vertical down.

macrographs of the cross-section of the weld beads performed under constant current and pulsed current, separated by average current value and by welding position (A: vertical up, P: flat; D: vertical down; S: overhead). Figure 4 shows the shape factor depending on the welding position and current, while Figure 5 illustrates the penetration depending on the welding position. Figure 6 shows stills from tests in the four welding positions, where we can see the different positioning configurations of the electric arc in relation to the weld pool and the filler wire.

As expected, the higher the welding current, the higher the values of the geometric characteristics obtained (Figure 3), such as width and bead reinforcement, linear penetration, penetrated zone (fusion zone of the base metal), linear reinforcement, reinforcement zone and heat-affected zone (HAZ). This can be explained by the increased amount of energy applied to the part in the form of heat, as well as the increased quantity of filler metal, since the wire speed/Power ratio was not modified during tests.

Welded beads in the vertical up and overhead positions display a lower shape factor (Figure 4) than the other welding positions. This is even more obvious when we look at the macrograph of the beads with lower welding voltage values. The low wettability in the vertical up position can be explained by the fact that the weld pool drains in the opposite direction to the solidification front, while in the overhead position, the weld pool drains away from the base metal (Figure 6).

In the overhead position, the beads created have greater reinforcement (reinforcement zone equal to length), resulting in a lower shape factor (Figure 4), which was an expected characteristic owing to the way the weld pool drains under the force of gravity in this position. In addition, when comparing the constant current with the pulsed current, as a general rule, the beads created with the pulsed current have a larger reinforcement zone. This is due to the fact that, with the same average current, the process with pulsed current requires more filler wire, which is noticed in data acquisition.

The position that has the highest linear penetration values (Figure 5) is vertical up. In this position, the weld pool drains in the opposite direction to the welding speed, which means that the arc is connected to the base metal more directly. This behaviour is displayed in Figure 6. This can be compared with the vertical down position, where the pool drains in the same direction as the welding speed, where the arc is directly connected to the pool, which means that the metal that is still solid receives less heat from the arc.

Figure 7 shows the microstructure of the base metal (BM) and the fusion zone (FZ), taken from the central area of each of the zones to be taken as representative. The microstructure of the BM consists of equiaxed grains of ferrite and fine pearlite, indicating that the material underwent final normalization. The fusion zone has a microstructure of allotriomorphic ferrite grains (primary ferrite or grain boundary ferrite – α_a), with acicular ferrite (AF) and Widmänstatten ferrite (ferrite with aligned second phase – α_W). These microstructures are typically observed in the fusion zone of low-carbon steels [13–16]. The acicular ferrite usually means that the toughness of the welded joint is increased [14], lending the weld metal good mechanical properties [13]. When comparing the micrographs of the fusion zone of samples welded in the same position (flat) using constant current, but with different average current values (Figure 7 (c) and (d)), we can see a finer microstructure in the samples welded with a lower current (120 A), and a greater presence of primary ferrite in the samples welded with a higher current (160 A), whereas in the sample with 120 A, there is a greater presence of acicular ferrite. The larger quantity of allotriomorphic ferrite (primary ferrite or grain boundary ferrite) is favoured by the slower cooling rate, as is the case for the welding current of 160 A [17].

For the pulsed current, the formation of acicular ferrite is even more pronounced, because this current generates a smaller heat input than the constant current, leading to a higher cooling rate. This is entirely consistent with existing literature [7,9], which justifies using pulsed current because the weld pool can be controlled better using this kind of waveform, primarily in welding out of the flat position. According to Grong and Matlock [13], the formation of ferrite initially grows from austenitic grain edges and boundaries under parabolic kinetics promoting the formation of the allotriomorphic structure, which has a carbon redistribution continuity which compromises this parabolic growth, enabling the lateral movement of protrusions along the low-energy interfaces, representing a Widmänstatten structure. Acicular ferrite can initiate nucleation with a similar mechanism to the Widmänstatten ferrite, i.e. intergranular nucleation on inclusions, at the same time as the formation of allotriomorphic/Widmänstatten structures. The predominant presence of AF is to be expected, given that the filler wire has a higher quantity of Mn than the base metal, which leads to a proportional increase in acicular ferrite [13].

Figure 8 contains images of the microstructure of the HAZ for samples welded in the flat position, with constant and pulsed current, taken from the central area of each of the zones to be taken as representative. According to Babu and David [14], Widmanstätten ferrite and acicular ferrite are formed by the same mechanism, but in different nucleation sites; Widmanstätten ferrite grows from allotriomorphic ferrite, while acicular ferrite nucleates in the interior of austenitic grain on inclusions. The microstructures found in the HAZ consisted of primary ferrite (allotriomorphic), ferrite plates (Widmanstätten) with aligned second phase (FS(A)) or with non-aligned second phase (FS (NA)), as well as acicular ferrite.

By analysing Figure 8, we can see that there is greater formation of allotriomorphic ferrite for the welding voltage of 160 A, whether constant or pulsed. As discussed above, the lower cooling rate for these samples encourages the formation of allotriomorphic ferrite and, consequently, ferrites with aligned second phase, FS(A) and ferrites with non-aligned second phase, FS(NA). We can also see more allotriomorphic ferrite with pulsed current than with constant current for the welding current of 160 A, which may be related to the faster cooling rate which, despite limiting allotriomorphic ferrite, leads to a smaller prior austenitic grain size providing, however, nucleation sites for allotriomorphic ferrite.

With the current of 120 A, we can see a mixed microstructure of second-phase ferrite plates and some acicular ferrite, which makes sense because the cooling rate is faster than for the welding current of 160 A and acicular ferrite is not encouraged. For the pulsed current, the smaller heat input and faster cooling rate lead to a smaller grain size and greater availability of nucleation sites for primary and acicular ferrites.

Figure 9 illustrates the Vickers microhardness values, obtained following a line of indentations on the base metal (BM) up to the fusion zone (FZ), passing through the HAZ, on six samples, three of which were welded with constant current and three of which were welded with pulsed current, all in the flat position. The hardness value of the BM was typically around 150 $HV_{0.5/15}$. The HAZ displayed slightly increased hardness starting from the interface with the BM and going up to the interface with the FZ, as was expected. The hardness values in the HAZ in the vicinity of the interface with the FZ (d = 4 mm) indicate that values are higher for the pulsed current of 120 A, which is consistent with the description of the microstructure of this section (with second-phase ferrite and acicular ferrite). With the constant current of 120 A, the hardness moderately decreases due to there being fewer nucleation sites for primary ferrite, which affects hardness. With the welding current of 160 A, we can see decreased hardness, which is related to the microstructure being predominantly formed from allotriomorphic ferrite and second-phase ferrite with the presence of some acicular ferrite.

In relation to the fusion zone, the greater hardness of the samples welded with pulsed current can be explained by the prevalence of acicular ferrite, compared with the

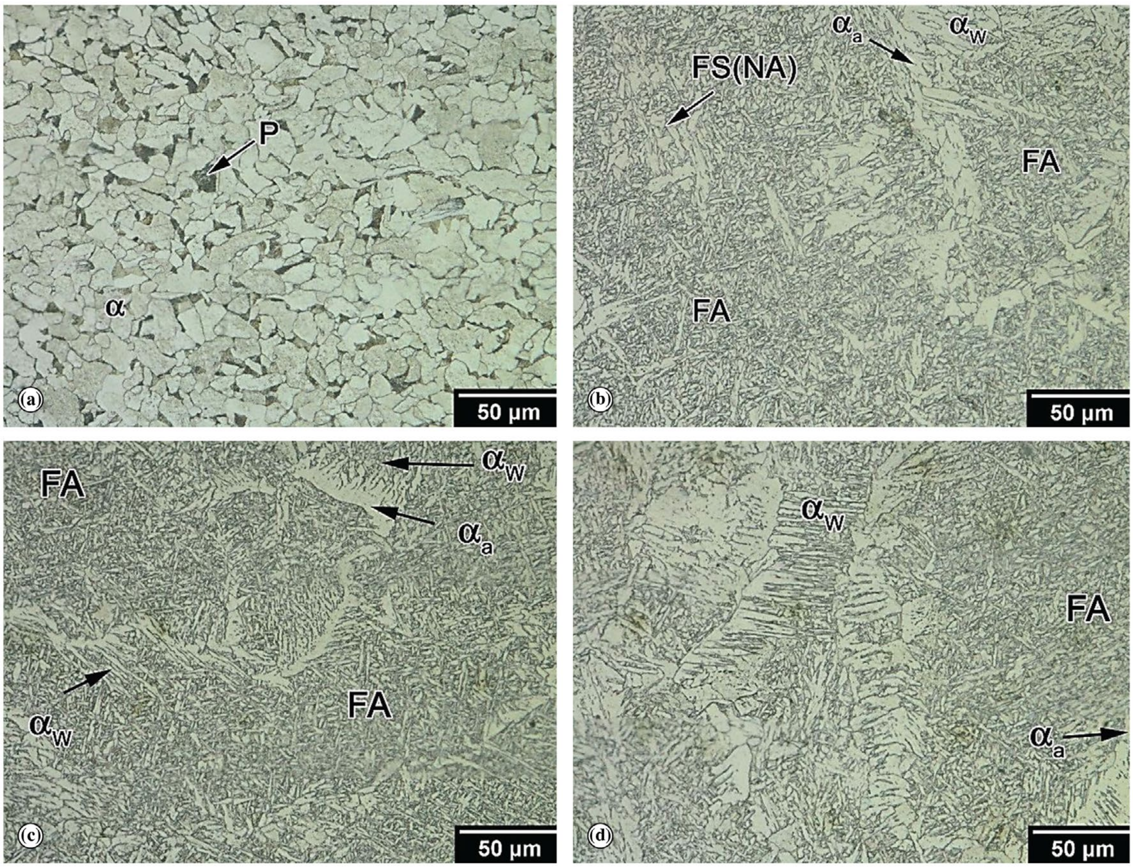

Figure 7. Microstructure of (a) the base metal, (b) the fusion zone with pulsed current of 160 A, (c) the fusion zone with constant current of 120 A and (d) 160 A for the flat welding position.

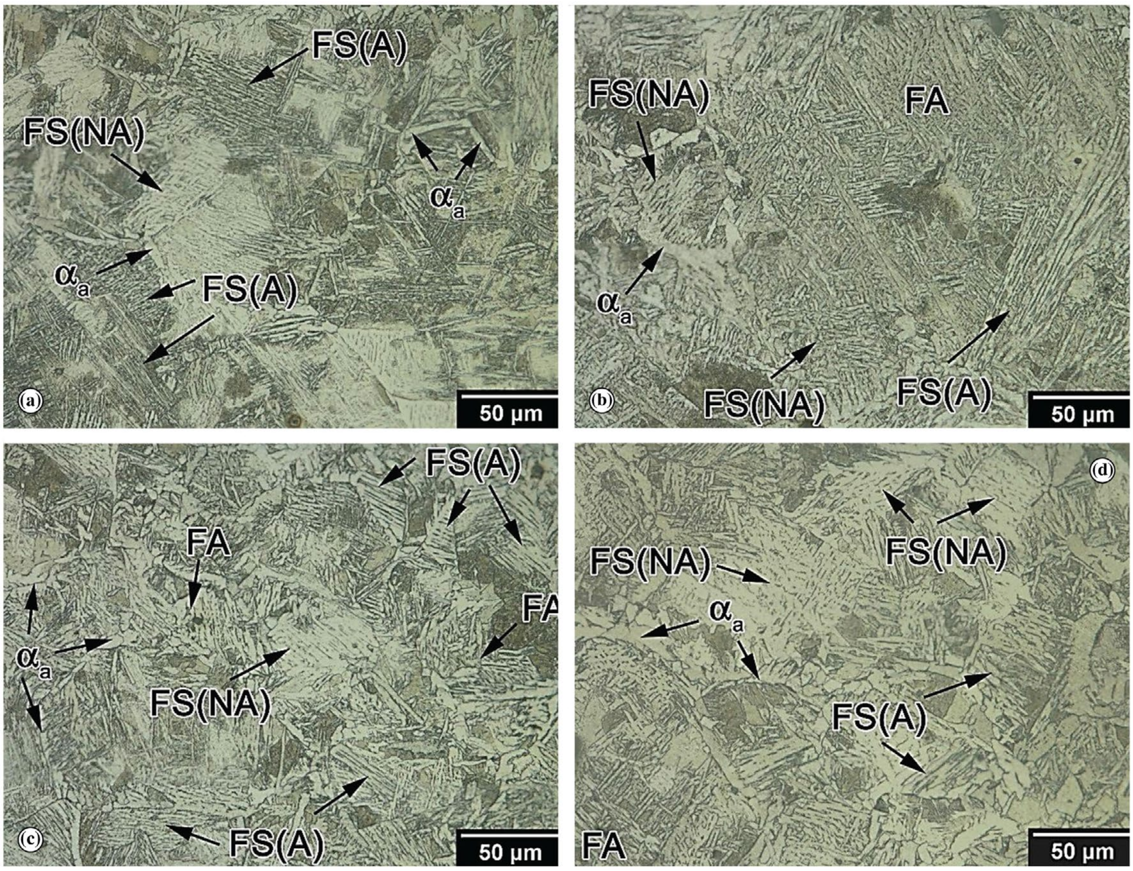

Figure 8. Microstructure of the HAZ for constant current of (a) 120 and (b) 160 A and for pulsed current of (c) 120 A and (d) 160 A in flat welding conditions.

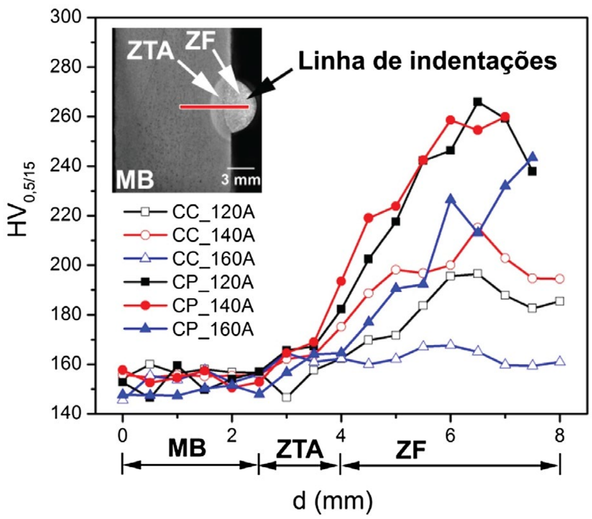

Figure 9. Hardness profile using microindentation starting from the base metal up to the fusion zone.
Notes: Linha de indentacoes: line of indentations. ZTA = HAZ; ZF = FZ; MB = BM; CC = constant current; CP = pulsed current.

constant current. By analysing the samples welded with the same waveform, we can see that hardness is greater in those with a lower welding current, due to the faster cooling rate, which leads to a finer microstructure, typically an acicular ferrite microstructure.

4. Conclusions

The continuous feed of metal was guaranteed with a ws/Pow ratio of the order of 1.2×10^{-5} m·J^{-1}, lending the process stability and providing a suitable shape factor.

The vertical up and overhead positions result in welds with a lower shape factor, owing to the drainage configuration of the weld pool under the force of gravity in these positions. For the same reason, beads welded in the vertical up position have greater linear penetration.

The fusion zone of samples welded with a lower current has a finer microstructure, with more acicular ferrite, while samples welded with a higher welding current have more allotriomorphic and Widmänstatten ferrite. In addition, the pulsed current encourages the formation of acicular ferrite, due to the smaller heat input compared with the constant current, leading to different cooling rates.

The microstructure consisted of second-phase ferrite, allotriomorphic ferrite and a smaller quantity of acicular ferrite in the case of the HAZ. There is a competitive effect with respect to the formation of allotriomorphic ferrite in the HAZ depending on the heat input; a smaller heat input resulting from pulsed current leads to a smaller prior austenitic grain size and therefore a larger grain boundary zone, which encourages the formation of allotriomorphic ferrite. On the other hand, welding currents of a lower magnitude also lead to a smaller heat input, increasing the cooling rate, which impedes the formation of allotriomorphic ferrite and encourages the formation of second-phase ferrite.

Acknowledgements

The authors would like to thank LABSOLDA/UFSC for providing the facilities for this work to be carried out, FINEP, ANP/Petrobras and CAPES for the financial support and scholarship.

Funding

This work was financially supported by the FINEP, ANP/Petrobras and CAPES.

References

[1] Agência Nacional do Petróleo, Gás Natural e Biocombustíveis. Anuário estatístico brasileiro do petróleo, gás natural e biocombustíveis [National Agency of Oil, Natural Gas and Biofuels. Brazilian annual volume of statistics for oil, natural gas and biofuels]. Rio de Janeiro: ANP; 2014.
[2] Carvalho RS, Dutra JC, Bonacorso NG. Desenvolvimento de um manipulador robótico para a soldagem orbital [Development of a robotic manipulator for orbital welding]. In: Rio Oil & Gas Expo and Conference; 2008 Sep 15–18; Rio de Janeiro. Rio de Janeiro: Brazilian Institute of Oil, Gas and Biofuels; 2008. p. 2–8.
[3] Cunha TV, Dutra JC. Desenvolvimento de um sistema de soldagem orbital de tubos: concepção do equipamento [Development of an orbital welding system for tubes: equipment design]. In: Anais do 4° Congresso Brasileiro de Pesquisa e Desenvolvimento em Petróleo e Gás; 2007 Outubro 21–14; Campinas [Annals of the 4th Brazilian Congress of Research and Development on Oil and Gas; 2007 Oct 21–14; Campinas]. Campinas: Associação Brasileira de P&D em Petróleo e Gás [Brazilian Association of Research and Development on Oil and Gas]; 2007.
[4] Lukkari J. Orbital-TIG – a great way to join pipes. ESAB Weld Cutting J. 2005;60(1):3–6.
[5] Ribeiro JCB, Silva RG. Desenvolvimento de procedimentos de soldagem TIG e análise de diferentes parâmetros para a soldagem de raiz em tubos de aço API 5L grau A [Development of TIG welding procedures and analysis of different parameters for root welding on API 5L grade A steel tubes]. In: Anais do 37° Congresso Nacional de Soldagem; 2011 Outubro 3–6; Natal [Annals of the 37th National Welding Congress; 2011 October 3–6; Natal]. São Paulo: Associação Brasileira de Soldagem; 2011.
[6] Sagues P. Adaptative control techniques advance automatic welding. Weld J. 2010:1–3.
[7] Latifi H. Advanced orbital pipe welding [doctorate's thesis]. Lappeenranta: Lappeenranta University of Technology; 2012.
[8] Pigozzo IO. Soldagem TIG orbital: otimização de equipamentos e prospecções tecnológicas para procedimentos de passe de raiz [dissertação de mestrado] [Orbital TIG welding: optimising equipment and technical prospecting for root pass procedures [master's dissertation]). Florianópolis: Universidade Federal de Santa Catarina; 2015.

[9] Fronius International GmbH. Orbital welding facts. Vol. 2. Wels: Polysoude Nantes Frankreich SAS; 2010. 52 p.

[10] Samardzic I, Despotovic B, Klaric S. Automatic pipe butt welding processes in steam boiler production. Weld World. 2007;51(7):615–624.

[11] Garcia JAO, Lima GL, Pereira WDB, et al. Advances of orbital gas tungsten arc welding for Brazilian space applications – experimental setup. J Aerosp Technol Manage. 2010;2(2):211–218. DOI:10.5028/jatm.2010.02026710

[12] Garcia JAO, Dias NS, Lima GL, et al. Characterization of titanium welded joints by the orbital gas tungsten arc welding process for aerospace application. J Aerosp Technol Manage. 2010;2(2):203–210. DOI:10.5028/jatm.2010.02026610

[13] Grong O, Matlock DA. Microstructural development in mild and low-alloy carbon weld metals. Int Met Rev. 1986;31(1):27–48.

[14] Babu SS, David SA. Inclusion formation and microstructure evolution in low alloy steel welds. ISIJ Int. 2002;42(12):1344–1353. DOI:10.2355/isijinternational.42.1344

[15] Hu F, Hodgson PD, Wu KM. Acceleration of the super bainite transformation through a coarse austenite grain size. Mater Lett. 2014;122:240–243. DOI:10.1016/j.matlet.2014.02.051

[16] Santos TFA, Torres EA, Vilela JMC, et al. Caracterização microestrutural de aços baixo carbono por microscopia de força atômica [Microstructural characterisation of low-carbon steel using atomic force microscopy]. Revista Latinoamericana de Metalurgia y Materiales [Lat-Am J Metall Mater]. 2015;35(1):118–133.

[17] Leitner RE, McElhinney GH, Pruitt EL. An investigation of pulsed GTA welding variables. In: Proceedings of the 54th AWS Annual Meeting; 1973 Abril 2–6; Chicago. Chicago: AWS; 1973.